Time-resolved imaging in dense scattering media

Jenghwa Chang, Yao Wang, Raphael Aronson
Departments of Electrical Engineering and Physics, Polytechnic University, Brooklyn, NY 11201

Harry L. Graber, Randall L. Barbour*
Departments of Pathology and Biophysics, SUNY Health Science Center, Brooklyn, NY 11203

B. Das, J. Dolne, K. M. Yoo, R. R. Alfano
Mediphotonics Laboratory, Institute for Ultrafast Spectroscopy and Lasers
City College of City University of New York, NY 10031

* Author to whom inquiries should be addressed.

ABSTRACT

The ability to image at optical frequencies objects embedded in a dense scattering medium has been experimentally evaluated using a previously described Progressive Expansion (PE) algorithm. Optical backscatter measurements were performed in a limited raster-type scan using a colliding pulse modelocked (CPM) femtosecond laser operating at 620 nm and streak camera. Data were collected in the presence and absence of the embedded absorber (3 mm diameter bead) located at a depth not visible from the surface, smoothed and evaluated between 0-200 ps in steps of 36 ps, using an overlapping approach contained in the PE algorithm, which is based on a linear perturbation model. Results obtained demonstrate the sensitivity of reconstructed images to variations in source and detector locations in relation to the subsurface location of the absorber.

1. INTRODUCTION

The range of tomographic imaging methods available for clinical diagnosis has grown considerably within the past decade, with special emphasis on developing methods that do not employ ionizing radiation[1]. More recently, significant interest has grown in the possibility of tomographic imaging of tissues at near infrared frequencies[2]. Because photons propagating through tissue are intensely scattered, the image recovery problem is much more difficult than for methods which evaluate straight line signals (*e.g.*, x-ray CT). Since photons exhibit both wave and particle behavior, it is natural to consider the two general mathematical formulations which describe the interaction of photons with matter. These are the wave and transport equations, respectively[3]. As practical matter, a principal difference between these two formulations is the type of information required as input for solution of the inverse problem. For the wave equation, it is necessary to measure both the amplitude and phase of the electric field. The transport equation, on the other hand, requires only measurement of intensity of the radiation field. In the presence of sufficient scattering, the latter is frequently the only parameter measurable, as complete dephasing of the signal can occur, rendering measurement of the electric field impractical.

Over the past several years we have concentrated on developing various strategies for solutions to the optical imaging problem, based on solutions to the transport equation employing a linear perturbation approach[4-7]. These formulations can consider data derived from either steady-state, time-resolved or amplitude modulated laser sources[7]. A variety of numerical methods have been tested, including conjugate gradient descent (CGD), projection onto convex sets (POCS) and a multigrid method[8]. More recently, we have described a progressive expansion algorithm which employs a overlapping scheme that is similar to a layer-stripping approach[9]. In this report we have tested the validity of this method, using experimental data obtained using a CPM femtosecond laser and streak camera, as a function of different source and detector locations.

0-8194-1114-0/93/$6.0

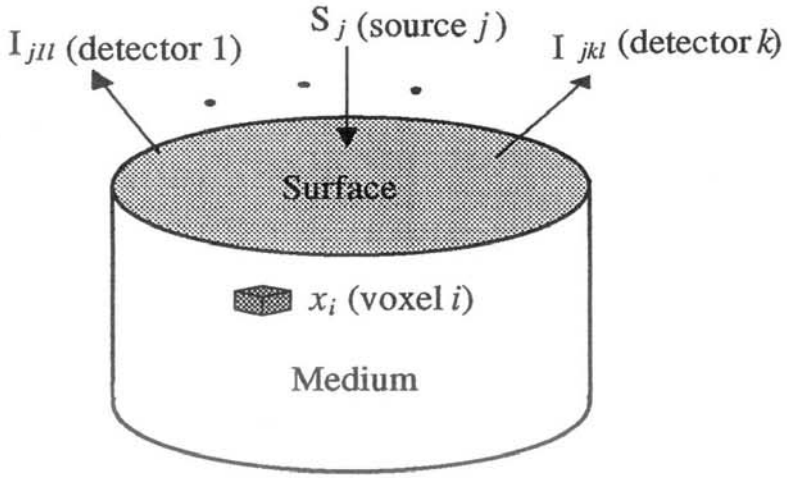

Figure 1. Illustration of the backscattering imaging problem. Photons are injected with intensity S_j (j = 1, 2, ..., J) at J source locations on the surface. For each source, K_j detectors were used to measure the temporal profile of the backscattered photon fluxes I_{jkl} (k = 1, 2, ..., K_j, and l = 1, 2, ..., L_{jk}) on the surface in L_{jk} time intervals. The problem is to reconstruct the absorption coefficients x_i from the time-resolved measurement I_{jkl}.

2. PROBLEM DESCRIPTION AND RECONSTRUCTION ALGORITHM

2.1 Problem Description

Consider a target medium in which photons are injected with intensities S_j at J source locations (j = 1, 2, ..., J) on the surface (see Figure 1). Photon fluxes I_{jkl} are measured in L_{jk} time intervals (l = 1, 2, ..., L_{jk}) at the kth detector (k = 1, 2, ..., K_j) for the jth incident signal. In this study, optical fibers were used to send and receive signals. The sources and detectors were placed on one side of the medium, and the backscattered field alone was measured. In the analysis of the data, the target medium was divided into N contiguous non-overlapping small volume elements, or voxels v_i, i= 1, 2, ..., N, each with its own scattering and absorption coefficients, s_i and x_i. The problem is to reconstruct the absorption coefficients x_i, i= 1, 2, ..., N of the media, from the time-resolved back-scattered measurements I_{jkl}.

2.2 Perturbation Approach for Diffusion Tomography

The perturbation model we have adopted (see reference 8 for detailed description) assumes that the absorption coefficients x_i of the unknown medium are very close to those of a reference medium, x_i^r. It relates the differences between the absorption properties of the two media, $\Delta x_i = x_i - x_i^r$, to the changes in detector readings, $\Delta I_{jkl} = I_{jkl} - I_{jkl}^r$, by the following first order approximation:

$$\sum_i w_{ijkl}\,\Delta x_i = \Delta I_{jkl},\ l = 1, 2, \ldots, L_{jk},\ k = 1, 2, \ldots, K_j,\ j = 1, 2, \ldots, J. \qquad (1)$$

Here, w_{ijkl}, which is determined by temporal convolution of the collision densities from the source j to voxel i and from the detector k to the voxel i, is called the *weight*[10], and specifies the reduction of the photon flux in time interval l at detector k due to the increase in absorption at voxel i when photons are injected from source j. The above equation can be represented in matrix form as:

$$\mathbf{W}\,\Delta\mathbf{X} = \Delta\mathbf{I}. \qquad (2)$$

2.3 Progressive Expansion (PE) Algorithm

The PE algorithm[9], which is similar to a layer-stripping approach, was developed for image recovery of time-resolved data. Similar to ultrasound imaging, this algorithm takes advantage of the time resolving ability of the detected signal to localize the information and simplify the reconstruction. The algorithm, previously described[9], is shown in Figure 2 and includes the following steps:

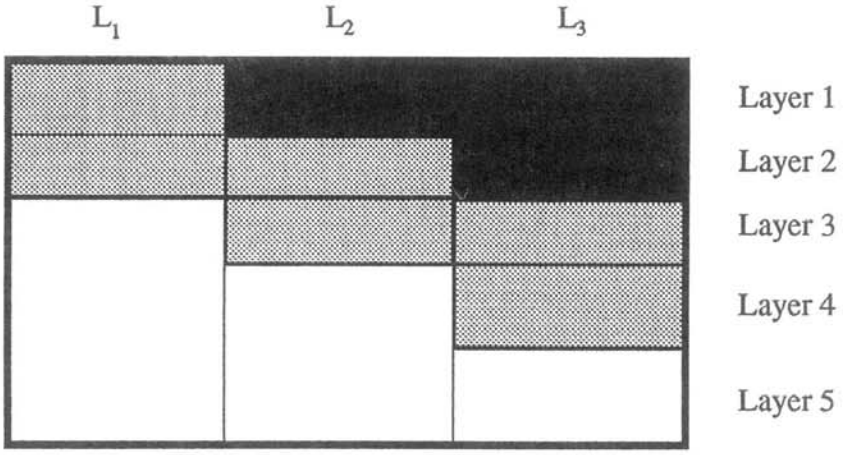

Figure 2. Illustration of Progressive Expansion Algorithm with overlapping scheme. This algorithm is similar to a layer-stripping approach, and takes advantage of the time-resolved property of the detected signal. In the first time interval, L_1, the first two layers were selected according to *Step 1* of the algorithm, and the reconstruction was performed. In the second time interval L_2, Layers 1, 2, and 3 were selected and the reconstruction were performed. The absorption coefficients of the first layer were fixed after the reconstruction. In time interval L_3, Layers 1, 2, 3, and 4 were selected according to *Steps* 1 and 2. Since Layer 1 was fixed after the previous reconstruction, its contribution to the detector readings were deducted according Eq. (3) of *Step 3*. After the reconstruction, Layer 2 was fixed , and the algorithm went to the next time interval.

Step 1. Find all the detectors which may receive signal during t_l by examining the weights of all the voxels for each detector. The number of detectors found is here denoted as m_l. The set of detector indices is denoted by U_l.

Step 2. Find all the non-fixed voxels which may contribute signal to any of the detectors determined in *Step 1* by including all voxels which have non-zero weights for at least one of the selected detectors. The number of voxels found is here denoted by n_l. The set of voxel indices is denoted by V_l.

Step 3. From the detector readings and voxels found in *Steps 1* and *2*, form the following set of linear equations:

$$\sum_{i \in V_1} w_{ijkl} \Delta x_i = \Delta I_{jkl} - \sum_{i \in V_1, \ldots, V_{l-1}} w_{ijkl} \Delta x_i, \quad j,k \in U_l, \text{ or } \quad \mathbf{W}_l \Delta \mathbf{X}_l = \Delta \tau_l, \tag{3}$$

Step 4. Find the least squares solution of Eq. (3) for $\Delta x_i \in V_l$. In our study, the CGD method was used because of its relatively fast convergence.

Step 5. Apply the positivity constraint to the reconstructed values. This is accomplished by setting $\Delta x_i = 0$ if $\Delta x_i < 0$.

Step 6. Fix $\Delta x_i \in V_l$. Go to the next time interval.

The advantages of this algorithm are: (a) it effectively reduces the matrix size, which has the effect of speeding up the reconstruction; (b) the matrix elements are more uniform, so the problem was better-posed. The disadvantages are: (a) it may be sensitive to noise if the time windows are too small; (b) the error from early reconstruction stages may propagate to later ones and introduce errors.

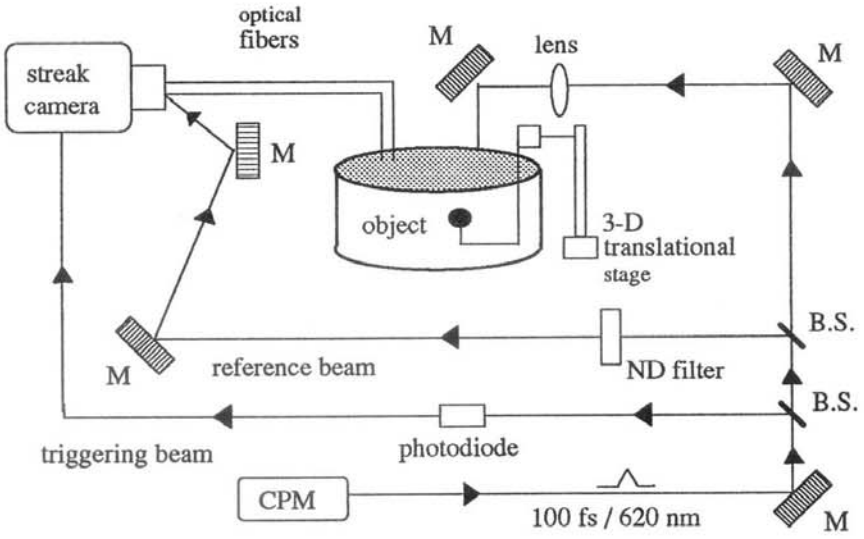

Figure 3. Experimental setup. (See text for description)

3. EXPERIMENTS

3.1 Experimental Setup

The experimental setup is shown in Figure 3. A CPM femtosecond laser was used to generate ultrafast (100 fs) laser pulses at 620 nm, which were divided into three beams. The first beam, directed to a photodiode, was used to trigger the streak camera. The second beam, which was reflected by two mirrors and reached the camera later, was used as the reference signal to normalize the readings to the same incident intensity. It was crucial to be sure that all readings were normalized, since the differences between readings of reference media and target media were used in the perturbation model. The third beam was directed to the reference and target media, and the backscattered light was collected by a 400 μm diameter fiber which entered the streak camera.

A 3 mm diameter black bead was used as target absorber. It was submerged into the water tank filled with diluted milk (10% whole milk, 90% water), and located 5 mm below the surface (Figure 4). At this depth, the bead was not discernible by eye in room light. The target medium was illuminated at eight different positions (1) - (8) as shown in Figure 4. For each illumination, four detector locations, (A), (B), (C) and (D), having the indicated separation, were used to collect data. To

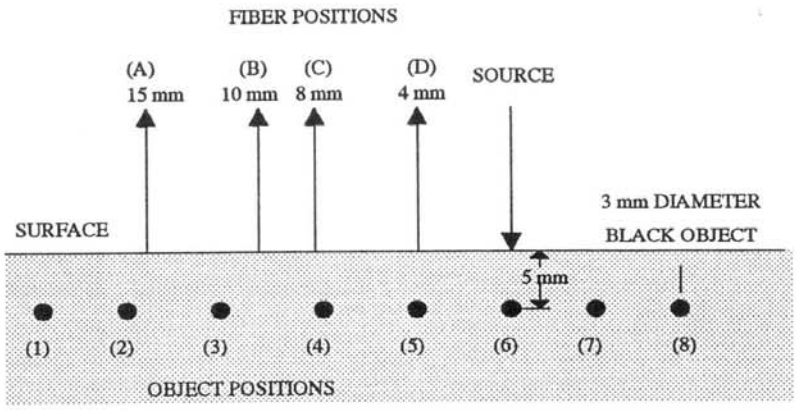

Figure 4. The source, detector and absorber positions for the experiment shown above. A 3-mm-diameter absorber was put at eight different positions (1) - (8) in the reference media. Four detectors (A), (B), (C), and (D) were used for each absorber

improve the S/N ratio, temporal profiles, which have a temporal resolution of approximately 4 ps, corresponding to each detector location were averaged for up to 15 seconds, which would correspond to 1000 pulses.

4. IMAGE PROCESSING

4.1 Preprocessing of Data

The preprocessing step operates on the raw data to filter out noise and normalize the data. Four steps were used in the preprocessing:

Step 1: Interpolate data to select time points.

Step 2: Normalize the data. The criterion for normalization is that the area under the reference signal is set equal to one; this effectively equalizes the same number of photons injected into the media for each temporal profile.

Step 3: Calculate difference, $I_0 - I$, where I_0 is the signal intensity for the reference medium and I is the signal intensity for the target medium. This will give ΔI for the perturbation model.

Step 4: Relate difference values from the absolute time scale used in the experiments to the distance time scale used in image reconstruction, that is, from picoseconds to mean free times (mft), where 1 mft = time for photon to travel 1 mean free path (mfp). In this study, 1 mft = 9.05 picoseconds. This conversion was necessary in order to use a step size consistent with that used in computing the weight functions.

4.2 Image Reconstruction

The layer-stripping algorithm described in Sec. 2 was used for image reconstruction. In this study, the reference and target media were modeled as a 41×41×10 mfp^3 region divided into 16,810 1×1×1 mfp^3 voxels (Figure 5). For each voxel, the weight function was calculated by convolving the source-to-voxel and detector-to-voxel (*i.e.*, photons are injected into the medium from the detector) collision densities in the reference medium over the selected time interval, which is 4 mft in this study. The collision densities in the reference medium were calculated beforehand using Monte Carlo simulations[10]. The reconstruction was performed on the Kilonode parallel computer at Syracuse University. The parallel computing was performed by splitting the program into different parts which were distributed to different nodes.

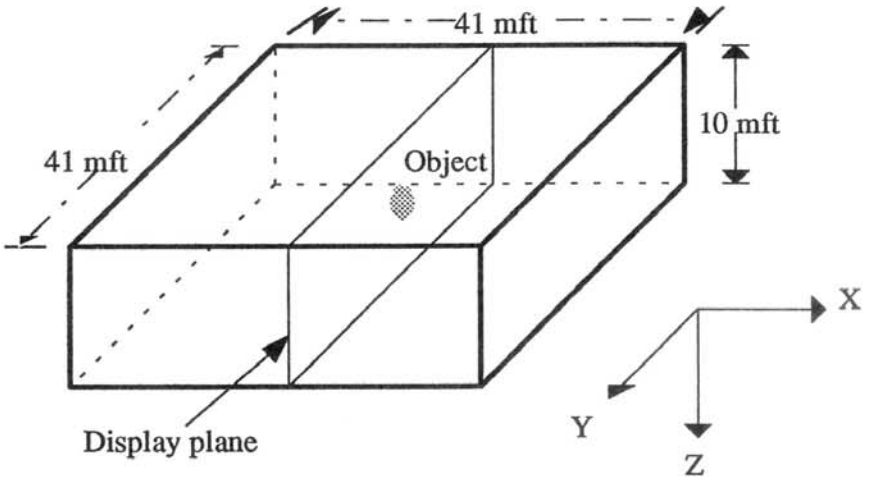

Figure 5. Mathematical modeling of the media for image reconstruction. The media were modeled as a 41x41x10 mfp^3 region, and divided into 16,810 1x1x1 mfp^3 voxels. A Euclidean (X-Y-Z) coordinate system was given as a reference, with X ranging from 30 to 70 mfp, Y from 30 to 70 mfp, and Z from 1 to 10 mfp. The position of the absorbing object was 3 mfp under the center (50,50,1) of surface as shown in the figure. Only the reconstruction result of the central plane (X = 50) was displayed.

The source positions are shown in Figure 6 and all the detectors in Figure 4 were used. Different combinations of source-detector pairs were tested, and the results are shown in Sec. 5.

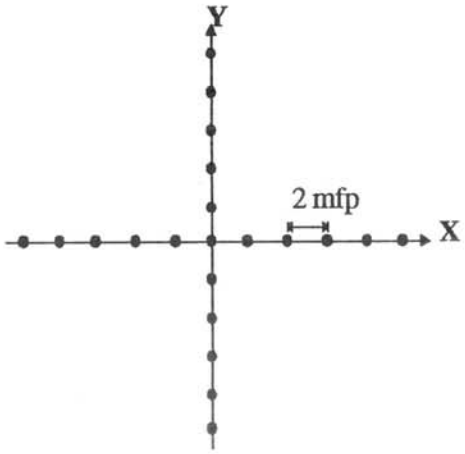

Figure 6. Source positions used in this study. From the source, detector, and absorber positions of Figure 4, the absorber was put in eight different positions. Equivalently, we can say that the absorber was fixed and the source was moved toward either direction, in 4 mm steps, which correspond to 2 mfp (mean free path) since the mfp in this study is 2 mm.

4.3 Display

Only one planar cross-section, as pointed out in Figure 5, is displayed for each reconstruction result, although the whole three dimensional structure was reconstructed. In our model, each cross-section plane was 41x10 mfp^2.

5. RESULTS

5.1 Results for Preprocessing

Figure 7 shows one of the temporal profiles of a detected signal. The source was located directly above the object, and the detectors were positioned at different distances (15 mm, 10 mm, 8 mm, and 4 mm for detectors A, B, C, and D,

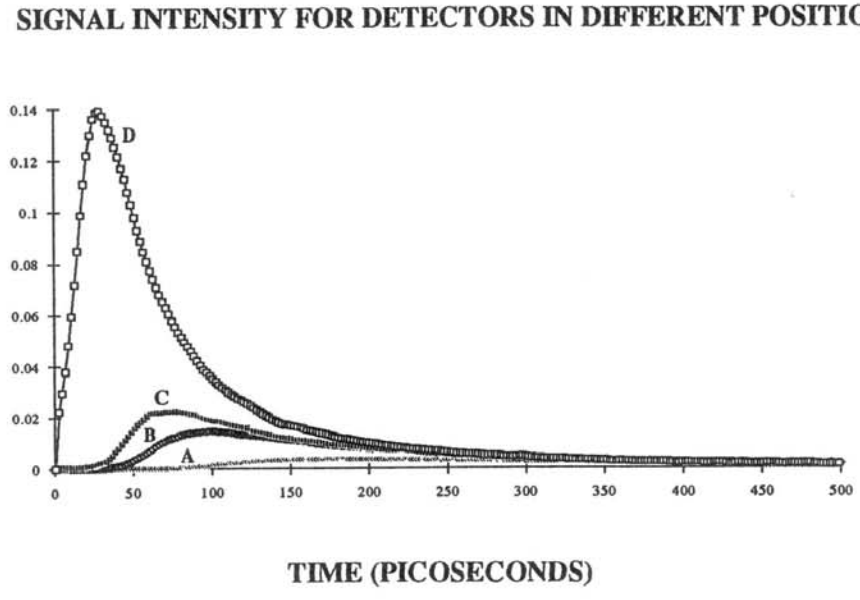

Figure 7. The temporal profiles for different detector locations. The source was located at the center of the surface, and the detector was located at 4 mm, 8 mm, 10 mm, or 15 mm from the source. Detector D, which was closest to the source, showed the strongest signal and an early, rapidly rising peak, while detector A, which was farthest form the source, has the weakest signal and a late, slowly rising peak.

respectively) from the source. Detector D, which is closest to the source, has the highest peak and earliest rising time, while detector A, which is farthest from the source, has the weakest signal and latest rising time. This is as expected, since the photons travel at a finite speed of light in the medium.

Figure 8 shows I_0 - I at detector A for different absorber positions. As expected, the differences are a function of absorber location.

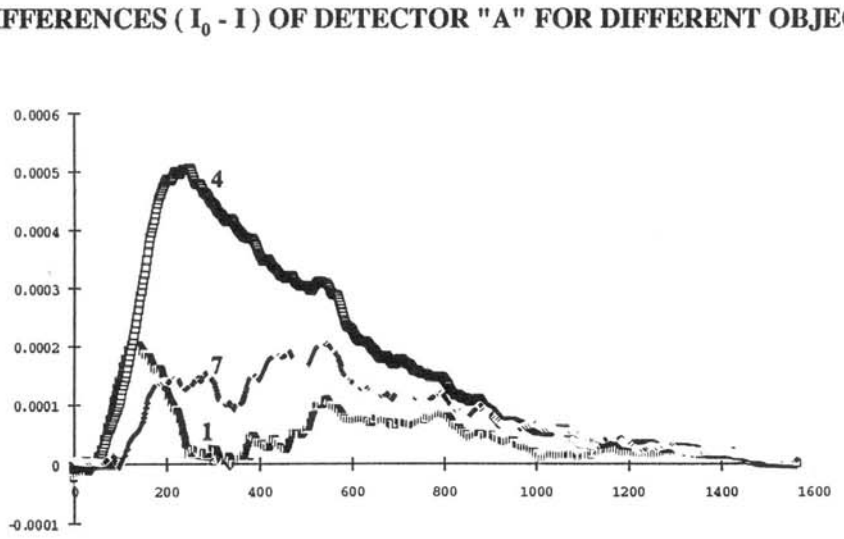

Figure 8. The temporal profiles of signal difference I_0 - I of detector A for three different absorber positions. The source was located at the center of the surface and the absorber was located at positions (1), (4), and (7) in Figure 4, respectively.

5.2 Results for Image Reconstruction

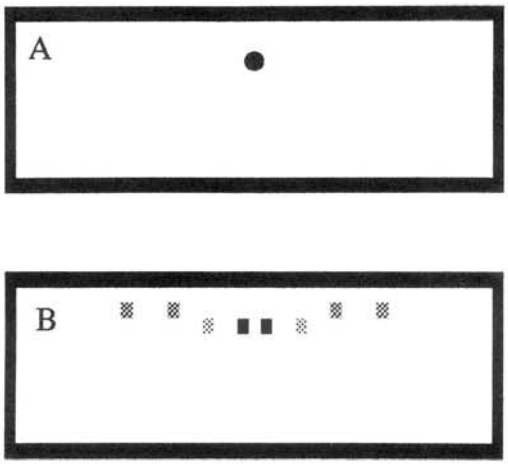

Figure 9. Reconstruction result with the source-detector pairs shown in Fig. 4 and 6: (a) the circle shows the actual position and size of the absorber; (b) the reconstructed image shows a doughnut-like ring surrounding the object. The location of the absorber is essentially correct. Some artifactual effects were observed with intensities relatively lower than the center. The image intensity is one tenth of the central point for the artifacts near the center, and one half for the artifacts on the edge.

Image reconstructions were carried out using data from different subsets of the total set of detector readings. Figure 9 shows the reconstruction result with the source-detector pairs shown in Figures 4 and 6. The shaded circle is the actual position, and the reconstructed image shows a doughnut-like ring surrounding the ball. The image is not perfect, but the location of the absorber is essentially correct. While some artifacts are present, their intensities are relatively lower than those in the "doughnut." The image intensity of the artifacts near the center and on the edge is one-tenth and one-half, respectively of the image intensity of the "doughnut".

Figure 10 shows a series of reconstruction results using detectors in different positions - only detector D was used in Figure 10A, detectors D and C in Figure 10B, detectors D, C, and B in Figure 10C, and detectors D, C, B, and A in Figure 10D. The result in 10D is exactly the same as Figure 9, which was used as a standard for comparison. In Figure 10A, for which only the nearest detector was used, the central doughnut is blurred and the artifacts have a higher relative intensity. As the number of detectors increases, the reconstruction results become closer to the standard.

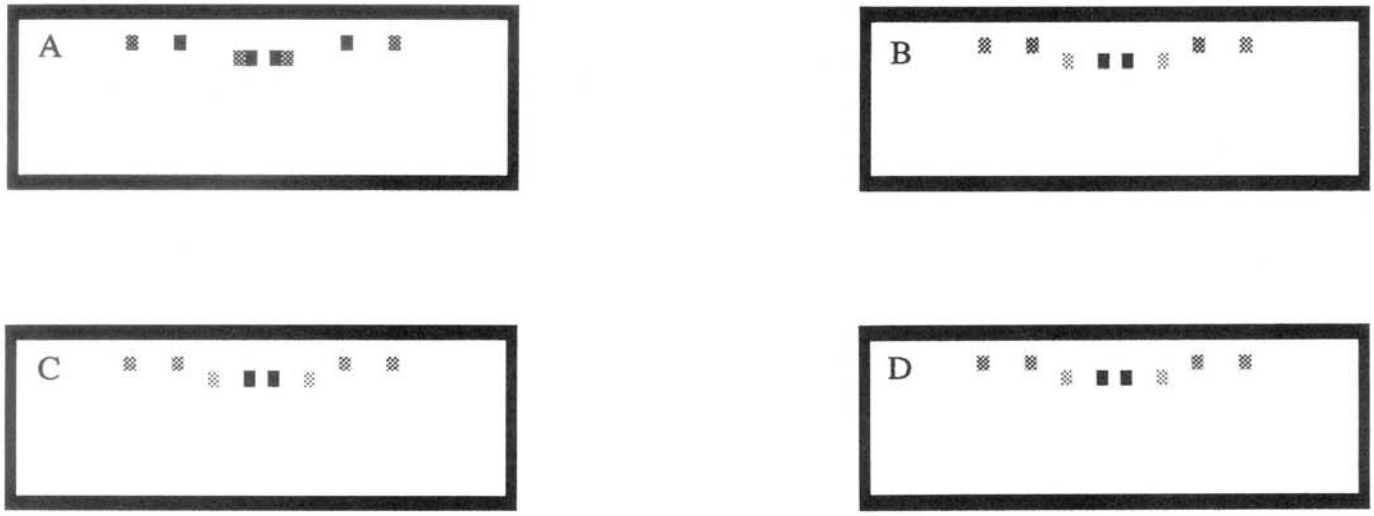

Figure 10. A series of reconstruction results with different detector positions: (a) only detector D was used; (b) detectors D and C were used; (c) detectors D, C, and B were used; and (d) detectors D, C, B, and A were used and the reconstruction is exactly the same as Fig. 9 which was used as a standard for comparison.

Figure 11 shows the reconstruction results for each single detector, *i.e.*, only detector D was used to obtain the result in Figure 11A, detector C in Figure 11B, detector B in Figure 11C, and detector A in Figure 11D. Only Figure 11A shows results which are similar to the standard. The image was blurred and the position of the doughnut was one voxel higher than in the standard. The other results were completely incorrect. This shows that the detectors which are closer to the source carry more information about the interior structure of the medium than do those which are farther away from the source.

Figure 12 further confirms this point. In this Figure, the detectors were sequentially removed, beginning with those nearest the source. As expected, when the innermost detectors were removed (Figure 12B), image quality begins to degrade, but some reasonable images were still obtained. When the nearest two detectors were removed (Figure 12C), the reconstruction results showed only random noise and were not acceptable. Results in Figure 13 show the sensitivity of image quality to removal of the source just above the object. Interestingly, these results indicate that the more distant detectors provide proportionally more information than when all the sources were considered. In Fig. 13a, the source just above the absorber was removed and only detector D was used for each remaining source. The ring surrounding the absorber was larger in the reconstruction, and its image intensity was lower than that of the artifacts. As detectors farther

from the source were sequentially added, the images improved and became closer to the standard. However, the image that incorporates all the detectors is still blurred and the intensity of the artifacts is greater than that seen in the standard. These results thus show that the source, as well as the detectors positions, have an impact on the image reconstruction.

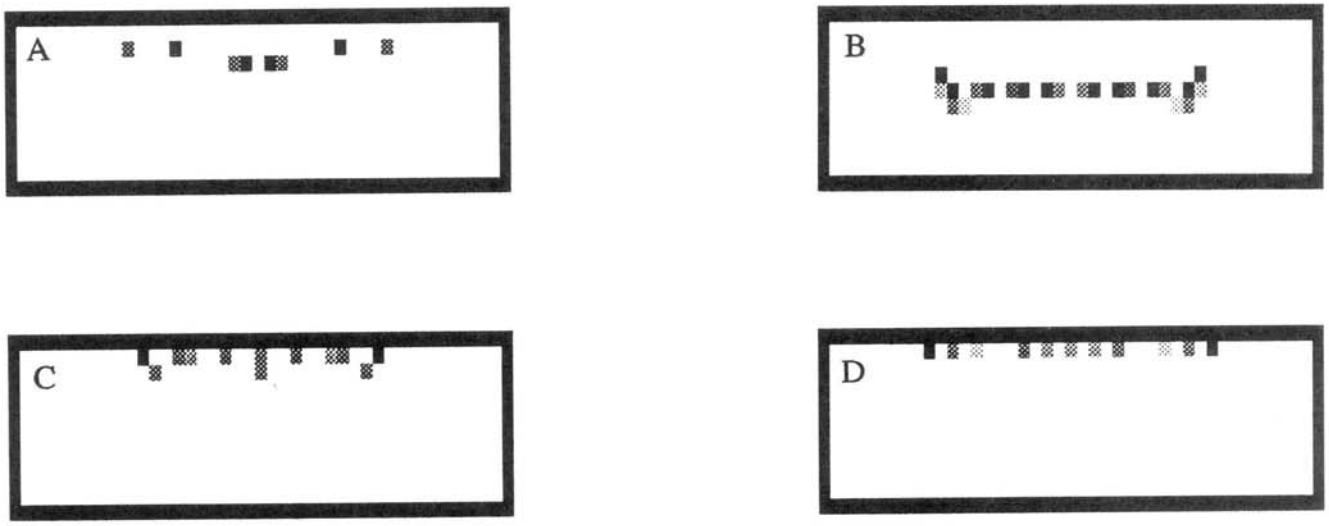

Figure 11. The reconstruction results for each single detector: (a) with detector D; (b) with detector C; (c) with detector B; (d) with detector A.

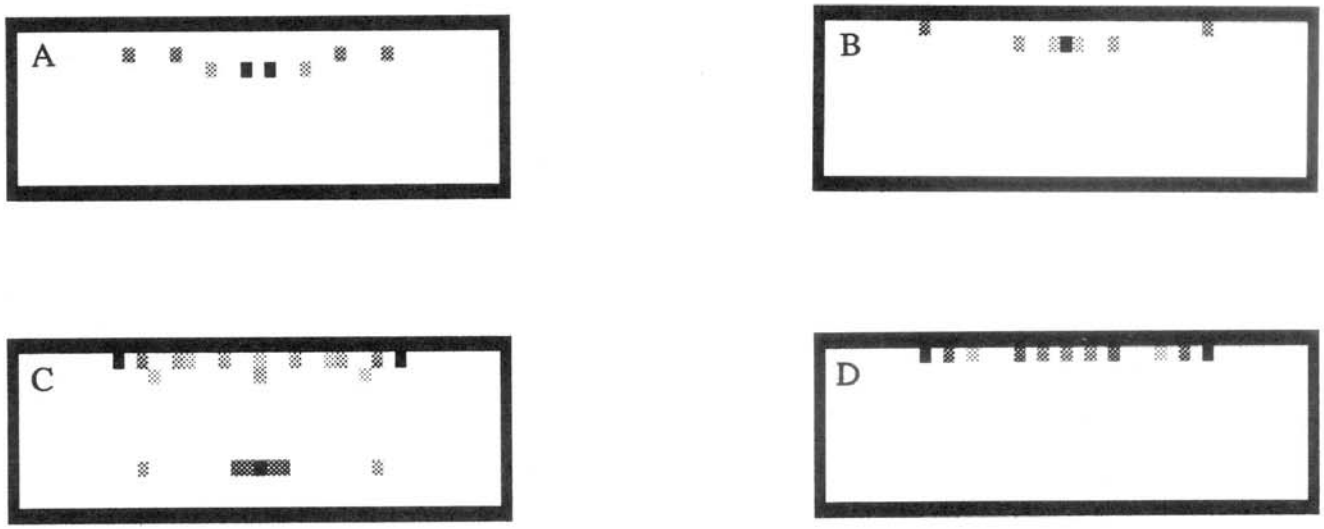

Figure 12. Reconstruction results for all sources but different detector positions: (a) all detectors A, B, C, and D were used; (b) detectors A, B, and C were used; (c) detectors A and B were used; (d) only A was used.

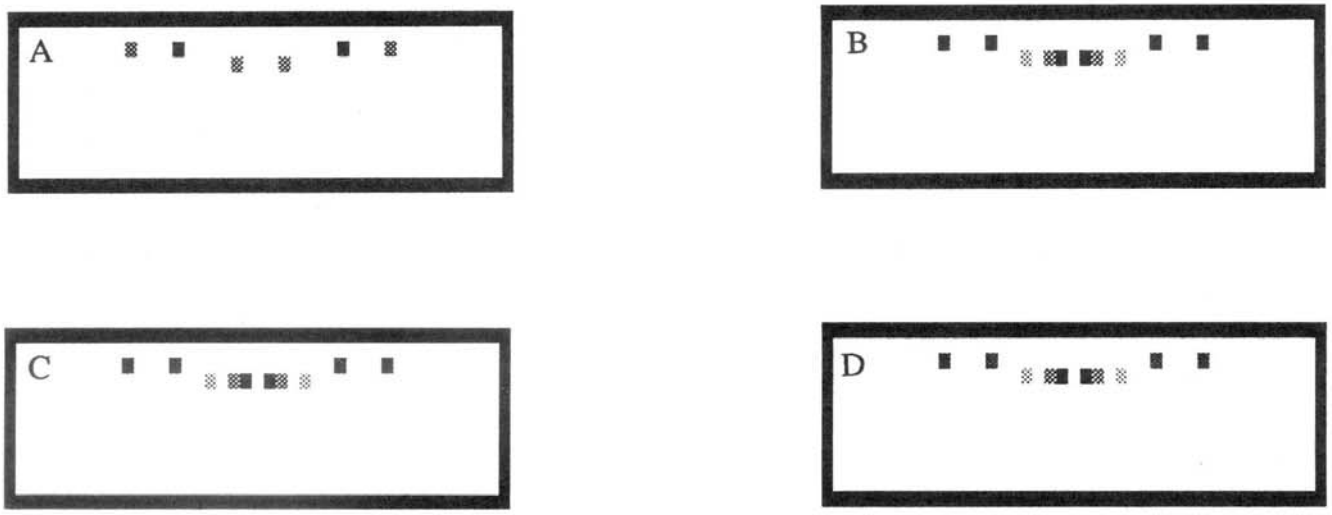

Figure 13. Reconstruction results for all sources except the one just above the object, with different detector positions (a) only detector D was used; (b) detectors D and C were used; (c) detectors D, C, and B were used; (d) all detectors D, C, B, and A were used.

6. DISCUSSION

The ability to image the interior of opaque media that scatter penetrating radiation holds the potential for greatly expanding the application range of imaging methods. It would allow, for example, the use of alternative energy sources previously considered unsuitable because of intense scattering experienced by penetrating photons. Because scattering represents an averaging effect, its occurrence complicates the image recovery problem by convoluting spatial information. From the perspective of the detector, it reduces the sensitivity to a given volume in the target medium. It follows that as the magnitude of scattering increases, an increasingly higher S/N ratio will be required to achieve a similar sensitivity to this specified volume. The influence of scattering can be reduced by employing time-resolved methods. At the earliest times, emerging photons have experienced the least amount of scattering and are therefore least sensitive to the above concerns. The relationship between photon transit time and path length lends itself to considering use of layer-stripping schemes. The progressive-expansion algorithm described here and elsewhere[9] basically employs this approach, by evaluating data corresponding to successively later emergence times in an overlapping scheme. Choice of the overlap interval involves tradeoffs between minimizing computing time and propagation of errors. This scheme can also be adopted to evaluate time-independent data. In this case, the analysis would proceed by considering, in a successive manner, the family of source-detector pairs located at increasing distances from a source.

An important issue partially examined here has been to evaluate image quality as a function of different locations of the source and detector in relation to each other and to the subsurface target, for a backscatter measurement. For the most part, a nearly coincident position of source and detector provided the greatest information of the subsurface, except when the target lay off the axis of the incident beam, in which case detectors located at greater distances from the source also provide useful information.

In this report, as in others[6-10], we have invoked the assumption of linearity with respect to the influence that absorption in the medium has on the response of surface detectors. Strong absorption will violate this assumption, causing an overestimate of weight in regions of a shadow. While it is expected that such errors will influence the resultant image, our experience has been that these effects are relatively small, at least for the case of a single inclusion and measurements

about the target vessel[7]. Because measurements reported here were limited to the backscatter field, the limited view angle may have contributed to the observed errors in reconstruction. Alternatively, the observed error may have resulted from the underdeterminedness of the data set. Regardless of which explanation, if any, is correct, the observed errors were relatively minor, as the "doughnut" was located at the correct horizontal and vertical position. This observation supports other findings from our group that one step of the linear perturbation model may be adequate for image recovery in some applications, at least for simply structured media[7]. For complex media, such as tissue, it seems likely that a scheme involving iterative updates of the weight matrices would be required for optimal image quality. Brute-force computations of the forward problem to recompute the weight matrices for each iteration would be prohibited, due to practical limits on computing time. An alternative approach would be to compute the non-local effects that regions of strong absorption have on the surrounding medium by identifying the histories of those photons principally affected. This computation would be tractable, in an iterative scheme, given an initial set of photon histories that identified the subsequent collision density of photons arising from each voxel in the medium for photons launched from the source, truncated to a preset threshold level. For a medium containing 30,000 voxels, the initial computation would require scoring the square of this number, or 9 $x10^8$ elements. While this number is large, a truncated set might only require considering a data set 5% as large a figure that current computing capabilities could easily handle. This "correction matrix" could then be used to compute the expected reduction in collision density throughout the medium for each source-detector pair, given an initial estimate of the strength and location of subsurface regions of absorption. The essence of this scheme would be to apply a first order, nonlinear correction to the weight matrices. It is recognized, though, that the impact of multiple strong absorbers in the medium will likely not depend strictly on the linear sum of the effect that individual strong absorbers have on collision density throughout the medium, as absorption at one site will influence the collision density at other sites.

The anticipated need to update the weight matrices in some fashion underscores the general characterization that the problem of image recovery of highly scattering media is unavoidably a large-scale computing problem. The accompanying reports in this volume by Schlereth *et al.*[4] and Klibanov *et al.*[11] explore other approaches to the inverse scattering problem. The prospect of coupling these schemes with the current one seems tenable and is currently being explored.

7. REFERENCES

(1) Other papers in this volume.

(2) *Photon Migration and Imaging in Random Media and Tissues*, vol. SPIE - 1888, (Los Angeles) eds. R. R. Alfano and B. Chance, 1993.

(3) A. Ishimaru, *Wave Propagation and Scattering in Random Media,* Academic Press, 1978.

(4) F. H. Schlereth, H. L. Graber, and R. L. Barbour, "Recovery of Scattering Media Using a Neural Net Approach", SPIE vol. 1887, accompanying paper in these proceedings, 1993.

(5) F. H. Schlereth, J. M. Fossaceca, A. D. Keckler, R. L. Barbour, "Imaging in Diffusing Media with a Neural Net Formulation: A Problem in Large Scale Computation", in *Proc. Physiological Monitoring and Early Detection Diagnostic Methods* , vol. SPIE - 1641, (Los Angeles), pp. 46-57, 1992.

(6) R. L. Barbour, H. L. Graber, Y. Wang, J. Chang,, R. Aronson, "A Perturbation Approach for Optical Diffusion Tomography Using Continuous-Wave and Time-Resolved Data", SPIE, *Medical Optical Tomography- Functional Imaging and Monitoring*, Budapest, 1993, in press.

(7) H. L. Graber, J. Chang, R. Aronson, and R. L. Barbour, "A Perturbation Model for Imaging in Dense Scattering Media: Derivation and Evaluation of Imaging Operators", SPIE, *Medical Optical Tomography- Functional Imaging and Monitoring*, Budapest, 1993, in press.

(8) Y. Wang, J. Chang, R. Aronson, R. L. Barbour, H. L. Graber and J. Lubowsky, "Imaging Scattering Media by Diffusion Tomography: An Iterative Perturbation Approach," in *Proc. Physiological Monitoring and Early Detection Diagnostic Methods* , vol.. SPIE - 1641, (Los Angeles), pp. 58-71, Jan. 1992.

(9) J. Chang, Y. Wang, R. Aronson, H. Graber, and R. L. Barbour, "A Layer Stripping Approach for Recovery of Scattering Media from Time-Resolved Data," in *Proc. Inverse Problems in Scattering and Imaging*, vol. SPIE - 1767, (San Diego), pp. 384-395, Jan. 1992.

(10) R. L. Barbour, H. L. Graber, R. Aronson and J. Lubowsky, "Imaging of diffusing media by a progressive iterative backprojection method using time-domain data," in *Proc. Physiological Monitoring and Early Detection Diagnostic Methods* , vol.. SPIE - 1641, (Los Angeles), pp. 21-34, Jan. 1992.

(11) M. V. Klibanov, S. Gutman, J. Malinsky, R. R. Alfano, J. Chang, R. L. Barbour, "Consideration of solutions to the inverse scattering problem for biomedical applications, vol. SPIE - 1887, accompanying paper in these proceedings, 1993.